RESEARCH ARTICLE

A Robust NIfTI Image Authentication Framework Based on DST and Multi-Scale Otsu Thresholding

KAMRED UDHAM SINGH [1], **SURBHI BHATIA** [2], **ANKIT KUMAR** [3], **SANDEEP KAUTISH** [4], **ADARSH KUMAR** [5], **SHAKILA BASHEER** [6], **AND ALAA ALI HAMEED** [7]

[1] Department of Computer Science and Information Engineering, National Cheng Kung University, Tainan 701, Taiwan
[2] Department of Information Systems, College of Computer Science and Information Technology, King Faisal University, Al-Ahsa 36362, Saudi Arabia
[3] Department of Computer Engineering and Applications, GLA University, Mathura 281406, India
[4] LBEF Campus, Kathmandu 44600, Nepal
[5] School of Computer Science, University of Petroleum and Energy Studies, Dehradun 248007, India
[6] Department of Information Systems, College of computer and Information Science, Princess Nourah Bint Abdulrahman University, P.O. Box 84428, Riyadh 11671, Saudi Arabia
[7] Department of Computer Engineering, Faculty of Engineering and Natural Sciences, Istinye University, 34010 Istanbul, Turkey

Corresponding authors: Sandeep Kautish (sandeep.kautish@lbef.edu.np) and Surbhi Bhatia (sbhatia@kfu.edu.sa)

ABSTRACT Telemedicine has been intensely promoted in the present pandemic situation of COVID-19 to maintain a strategic distance from the infected person. Several medical tests were used to detect the coronavirus, including antigen, RT-PCR, and a lung CT scan. Only a lung CT-Scan can detect the coronavirus and provide information about the lung infection. As a result, digital imaging plays a critical role in the current pandemic situation. Teleradiology allows for the communication of digital medical images of patients over the internet for diagnosis. A lung CT-Scan test is currently being performed on billions of people to detect COVID-19. These images were sent via the internet for diagnosis and research purposes. The NIfTI image file (.nii extension) was created by the CT-Scanner and contains multiple slices of the lungs. As a result, radiologists determine that the received image has not been tempered during transmission, posing a critical authenticity problem when transmitting these images over the internet. As a result, the researchers are more concerned about the integrity and authenticity of these images in teleradiology. This paper proposes a blind, robust watermarking scheme for lung CT-Scan NIfTI images to address this issue. We use Otsu's image segmentation algorithm in the proposed scheme to identify the slice with the least amount of medical information for watermark embedding. The proposed scheme employs the Discrete Shearlet Transform (DST), Lifting Wavelet Transform (LWT), and Schur decomposition to embed the encrypted watermark. Watermarks are encrypted using the Affine Transform. The experimental results show that watermarked slice has been tainted by the addition of various sorts of noise, including salt-and-pepper noise, compression, Gaussian noise, speckle noise, and motion blur. After an attack, a watermark is retrieved, and the NC values of extracted watermarks are 0.99623 for Salt and pepper noise, 0.96964 for Gaussian noise, 0.99014 for Speckle noise. The proposed scheme was put to the test with a variety of attacks and produced significant results.

INDEX TERMS Watermarking, NIfTI, DST, medical image, LWT, lung CT-scan.

I. INTRODUCTION

This APID mutation in SARS-CoV-2 (severe acute respiratory syndrome coronavirus 2) creates trouble for the world's medical healthcare system. The current global epidemic of

---

The associate editor coordinating the review of this manuscript and approving it for publication was Yongjie Li.

COVID-19, which SARS-CoV-2 triggered, has resulted in the deaths of millions of people around the world [1]. The death toll is steadily rising, and the pandemic circumstance is intense. At this time, the epidemic has expanded to even more than 220 countries and territories worldwide. COVID-19 is around the world, and pandemic circumstance is seething fiercely throughout the globe. It has created a threat to the

health of over 80% of the world's population. Doctors and radiologists provide remote consultations and deliver medical services promptly. Through the use of remote consultation, medical professionals working in hospitals can monitor and control the infection's source, interrupt its transmission path, cut down on the risk of cross-contamination within the facility, and ensure that hospitals continue to operate normally. Teleradiology provides the digital transmission ability of radiological images and patient-related data from one location to another for primary diagnosis and interpretation [2]. The CT-Scan image of the lungs is used as the most direct and compelling test in detecting lung infection of the covid-19 patients in remote consultations. Babukarthik et al. Proposed a covid detection model using chest X-ray images based on Genetic Deep Learning Convolutional Neural Network architecture that includes Huddle Particle Swarm Optimization [37], [38]. Its correctness has a direct impact on the diagnosis of coronavirus. CT-Scanner generated the multiple slices of the lung and combined them in a single image file, i.e., NIfTI (Neuroimaging Informatics Technology Initiative) with the file extension. nii. That's why neuroimaging researchers have broadly accepted the NIfTI image format.

NIfTI file formats are of two NIfTI files: NIfTI-1 and NIfTI-2. The NIfTI-2 format is an advanced version NIfTI-1 format suitable for more data storage. In imaging informatics for neuroscience and even neuroradiology research, NIfTI files are frequently used [3]. The first three dimensions of the NIfTI format are used to specify the three spatial dimensions, x, y, and z, whereas the fourth is used to define the time points t. Other uses for the remaining dimensions include holding vector-based data or voxel-specific distributional parameters [4]. It is possible to compress NIfTI files. The deflate algorithm can compress and decompress data of the NIfTI file. Thus,.nii.gz is the extension of the compressed versions of the NIfTI image.

However, in today's complex network world, even minor distortions in medical images during transmission can significantly impact diagnosis, resulting in significant ramifications. Guaranteeing the integrity and authenticity of digital medical images is a critical matter faced by remote radiologists because some malicious attacks tampered with the images. Digital watermarking on medical images was introduced to protect medical images from tampering. Tampering with medical images can result in incorrect diagnosis and treatment, which can be life-threatening. The ROI (important area for diagnosis) and the region of noninterest (less important area for diagnosis) are usually the two regions in a medical image [5]. If the data of the ROI area is altered slightly, it can lead to a false diagnosis and even fatal consequences. As a result, even for minor tampering, the radiologist must recognize whether the received image has been tempered or not. A watermarking (authentication mark) is inserted in the host image. A watermark is a logo that contains information embedded in an image to prove its authenticity. Numerous watermarking schemes have been developed to preserve the

patient's information and the authenticity of the medical image [6], [7], [8].

Fundamentally, the process of extracting a watermark has been categorized into three classes. If the host image is needed, the procedure calls non-blind; if no other information is required, then the watermarking process is called blind. The additional information, including a histogram, statistical parameters, etc., is required for watermark extraction then, the watermarking scheme is called semi-blind. When developing a watermarking system, it is essential to consider these factors: robustness, imperceptibility, and capacity [9], [10]. A prominent aspect of these concerns is that all these features cannot be given concurrently.

Su et al. [11] presented a Slant transform-based scheme. This scheme inserts the watermark in the maximum energy coefficient using the adaptive bit insertion position. A scheme for DICOM images is developed by Singh et al. [12]. This scheme uses the LWT, LU decomposition, and MSVD to improve security and robustness. Firstly, they applied a lifting wavelet on the host image then the low-frequency LL band was subjected to MSVD. Before the watermark embedding, it is also subject to LU factorization, which creates the binary vector and inserts the LL band of the MSVD. Kumar et al. [13] propose a scheme using LWT and QR factorization for NIfTI images. The authors initially extracted the patient metadata and the slice data from the source image. Then select the slice from the NIfTI image and perform the LWT, and finally, QR decomposed watermark bits are inserted in the low-frequency band. Another scheme is suggested by Singh et al. [14] for NIfTI images. In this scheme author embedded the multiple binary watermarks in the slice of the NIfTI image. The authors additionally evaluated this approach against a variety of noise attacks. They claimed that it is resilient against all of them, even though they tested it against varying numbers of watermark insertions. Ernawan et al. [15] presented a scheme for medical images. In this method, initially, they divided the image into chunks, and then again, each chunk is subdivided, and the watermark is added to the LSB. Gao et al. [16] use a zero-watermarking technique for tensor images to generate the watermark image using the XOR operation on watermark information and feature image. Moad et al. [17] suggested a method for watermarking for secure telemedicine applications. They insert a watermark that contains the patient's image and information. This method uses DCT and embeds the watermark into the mid-frequency band. They have developed another algorithm for medical images [18]. In this scheme, three different transformations are used: DWT, Shearlet, and Contourlet Transform. After that, Schur decomposition is applied to each transform's selected bands. Finally, watermark bits are embedded into the upper triangular matrix. Another strategy that uses the Fast Walsh Transform (FWT), the SLT, and the SVD was proposed by Bamal and Kasana [20]. The NROI is also used to insert the watermark in this particular scheme. After applying Fast Walsh Transform to the NROI blocks, SVD to these blocks to insert the first watermark, and SLT

transform to insert the second watermark into the image's red channel, the first watermark has been inserted into the image. Dai et al. [19] develop a watermarking method for medical images using SVD and Slantlet Transform the select the slice of a lung CT scan and use it for watermarking. Li et al. [31] developed a medical image zero watermarking approach that uses accelerated KAZE DCT. Initially, they applied AKAZE-DCT to get the feature vector of the picture, and then they merged it with the perceptual hashing approach to get the feature sequence. Next, they apply logistic chaos on the watermark to obtain the encrypted watermark logo, which they inserted into the image and scheme is robust against the geometric attacks. Another scheme for medical images is presented by Liu et al. [32]; in the scheme, the authors increase the security of the watermark by combining the Tent chaos with the Henon chaos. They applied the ridgelet-DCT transform and extracted the medical image's feature vectors. Finally, this binary vector is embedded into the image as a watermark. This scheme is not robust against geometric attacks. The research by Zhang et al. [33] aimed to address the issues of a low embedding rate and poor visual quality of the watermarking system. The inverse histogram transform has been used in this method to embed the encrypted watermark within the image.

Kumar and Singh [34] proposed a Finite Ridgelet Transform and Hessenberg decomposition-based watermarking scheme. In the first step, they applied the FRT and divided it into 4×4 blocks. Then random shuffling is done on these blocks. Finally, Hessenberg decomposition is applied, and the watermark coefficients are embedded into the Q matrix using the additive quantization technique. Gong et al. [35] proposed a zero-watermarking algorithm for medical images using deep learning and DCT. They applied the DCT on the image and then applied the Residual-DenseNet to extract the high-level feature to create the hash vector. Finally, the binary form of this vector is used as a key to encrypt the watermark. After watermark generation, the encrypted watermark is embedded in the image. Another research by Horasan et al. [36] for medical image watermarking is based on SVD and RDWT. First, they applied the DWT, and the SVD applied over the LL band to obtain the singular value matrix. Finally, watermark bits are embedded in a singular value.

As we know, the CT-Scanner generates the NIfTI image, which contains several slices. Within the present health care system context, the CT slice counts that are most typically accessible are as follows: 16, 32, 40, 64, and 128 slices, whereas the CT scanners that provide up to 256 and 320 slices are less prevalent. The scanners generating between 4 and 8 slices are gradually being phased out of the medical imaging system. Thus, the slice selection with less medical information must be used for watermarking to avoid improper diagnosis. In over proposed scheme, we have tackled this problem.

A. KEY CONTRIBUTIONS

The proposed novel watermarking scheme for the lung's NIfTI images is based on Shearlet domain, LWT, Otsu's image segmentation, Schur matrix decomposition, and affine transform. This scheme intends to help the radiologist provide the correct diagnosis to the patient. Before starting the diagnosis of the image, the radiologist must verify the image's authenticity because the received image may have been altered or modified by the malicious attackers in between the transmission over the internet. The proposed scheme aims to improve the robustness counter to the attacks and provide the correct diagnosis. The following are the most significant contributions made by the research paper:

a. Use Otsu's image segmentation to identify the NIfTI image slice containing the least amount of medical information to embed a watermark. This means that the critical slices have been preserved, while only one slice with less information has been used for watermark insertion. As a result, the diagnosis of the NIFTI image must not be disrupted.
b. DST's multi-resolution and multi-direction capabilities can outperform rest transforms such as DWT and DCT.
c. Different strength levels for each direction of DST are used to improve robustness and imperceptibility.
d. LWT can resist signal distortion and assist in extracting watermarks with the highest possible, which improves security.
e. An affine transform is utilized to encrypt the watermark to assure the security of the embedded watermark.
f. The robustness and security of NIfTI images are provided by a hybrid combination of Otsu's image segmentation, DST, LWT, Schur decomposition, and affine transform. This scheme must ensure that the diagnosis will not be affected.

The remaining portions of this paper have been separated into the following sections: In Section 2, we discuss the overview of the theories that were used in the proposed scheme; in Section 3, we discuss the proposed approach to watermark insertion and extraction; in Section 4, conducts simulations and assesses simulation result; and in Section 5, concludes the desired study.

II. BACKGROUND THEORIES

A. NIfTI IMAGE

This file format was developed for neuroimaging image files in the early 2000s, which retains the benefits of the Analyze format while overcoming its shortcomings [3]. The NIfTI format can be considered an improved version of the Analyze format. NIfTI now supports data types that the Analyze format did not previously support, such as unsigned 16-bit. Image files are typically saved as a single.''nii'' file that contains both the header and the pixel data [21]. NIfTI file format is represented as $I \times J \times N$, where $I \times J$ represent the slice dimension, and the N represents the number of slices in the NIfTI file. In the paper, $512 \times 512 \times N$ have been used for the experiential purpose. Fig. 1 depicts the number of slices in each NIFTI image used for the experiment.
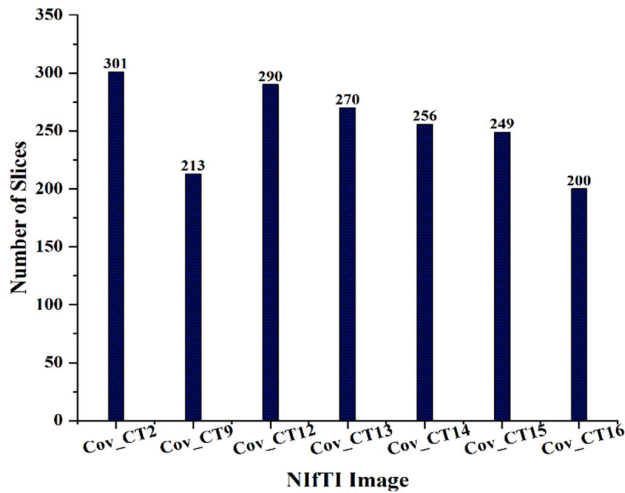
FIGURE 1. Number of slices in NIfTI images.

B. OTSU IMAGE SEGMENTATION

In 1979, Otsu developed a dynamic threshold selection technique. This technique proposes maximizing the weighted sum of between-class foreground and background pixels variances to determine an optimal threshold. Because the Otsu technique is simple, it has been extensively used in image segmentation [22], [23]. The fundamental OTSU-based threshold segmentation concept is stated as:

Assume that the range of the grayscale image is i = 0, 1,2,.........M-1 and the number of the pixels with grayscale g is n_g, then the total number of pixels T_p in an image

$$T_p = \sum_{g=0}^{M-1} n_g = n_0 + n_1 + \ldots + n_{M-1} \quad (1)$$

The probability of gray level g's occurrence is

$$p_g = \frac{n_g}{T_p} = \frac{n_g}{\sum_{g=0}^{M-1} n_g} \quad (2)$$

Threshold T of grayscale can be used to divide the gray level image into parts Q_1 and Q_2. Such that

$$Q_1 = (0, 1, 2, 3, \ldots t)$$
$$Q_2 = (t+1, t+2, \ldots M) \quad (3)$$

Probability and mean of the Q_1 and Q_2 are

$$Z_0 = P(Q_1) = \sum_{i=0}^{t} p_i = Z(t) \quad (4)$$

$$Z_1 = P(Q_2) = \sum_{i=i+1}^{M-1} p_i = 1 - Z(t) \quad (5)$$

Now the mean of the class Q_1 and Q_2 are

$$\mu_0 = \sum_{i=0}^{t} \frac{i * p_i}{Z_0} = \frac{\mu_t}{Z(t)} \quad (6)$$

$$\mu_1 = \sum_{i=t+1}^{M-1} \frac{i * p_i}{Z_1} = \mu_T - \mu(t)/1 - Z(t) \quad (7)$$

Were,

$$\mu_t = \sum_{i=0}^{M-1} i * p_i \quad (8)$$

$$\mu_T = \sum_{i=0}^{M-1} i * p_i \quad (9)$$

For any value of t $Z_0\mu_0 + Z_1\mu_1 = \mu_T$ is the total mean of gray level and $Z_0 + Z_1 = 1$

Now the variance of class Q_1 and Q_2 are

$$\sigma_0^2 = \sum_{i=1}^{t} \frac{(i - \mu_0)^2 * p_i}{Z_0} \quad (10)$$

$$\sigma_1^2 = \sum_{i=t+1}^{M-1} \frac{(i - \mu_1)^2 * p_i}{Z_1} \quad (11)$$

So, the interclass variance is

$$\sigma_z^2 = Z_0\sigma_0^2 + Z_1\sigma_1^2 \quad (12)$$
$$\sigma_B^2 = Z_0 (\mu_0 - \mu_T)^2 + Z_1 (\mu_1 - \mu_T)^2 \quad (13)$$
$$\sigma_B^2 = Z_0Z_1(\mu_1 - \mu_T)^2 \quad (14)$$

Then the overall variance of the gray level is $\sigma_T^2 = \sigma_Z^2 + \sigma_B^2$

Because the overall variance, that is, the sum of the within-class variance and the between-class variance, stays the same from partition to partition, this method select the optimal threshold T^* by maximizing the between-class variance. It is equivalent to minimizing the within-class variance since the partitioning unaffected overall variance.

$$T^* = Arg_{0<T<M-1}max(\sigma^2 (T)) \quad (15)$$

The above discussion shows that when σ_B^2 is at its maximum, the optimal threshold value T^* of T must be achieved.

C. DISCRETE SHEARLET TRANSFORM

The DWT is the most often employed transform in image processing applications. Although wavelets help one-dimensional estimate signals, they are inefficient for 2D or multi-dimensional data. The edges divide the smooth areas in the image containing two-dimensional (2D) smooth signal components because the edges are placed along smooth curves. 2D wavelets help separate edge point discontinuities but do not handle continuities along smooth curves. 2D wavelets are produced by tensor multiplication of 1D wavelets [24]. As the scale is reduced, the quantity of these expressions rises, revealing the wavelet's vulnerability. However, sparse and optimum modes depict this border and curve in multi-directional wavelets.

The Discrete Shearlet transform (DST) is a discrete representation for multi-scale directionality that combines the ability to use multi-scale techniques and capture the geometry of multi-dimensional data. DST is fundamentally an affine system that uses a single mother Shearlet function specified by three parameters: scaling, translation, and shear. The shear parameter is used to specify the directions of the various singularities [25]. For the image I, its mapping is described as follows:

$$I \rightarrow SH_\Psi I (a, s, t) \quad (16)$$

The three parameters a, s, and t, represent scale, shearing, and translation, respectively, where a > 0 and s ∈ ℤ. The Shearlet transform can be written as:

$$SH_\Psi I (a, s, t) = \int (t')\Psi_{as} (t - t') dt' = I.\Psi_{as} (t) \quad (17)$$

The Shearlet coefficients are computed by dilating, shearing, and translating. Shearlet coefficients can be given for each mother function, as follows:

$$\Psi_{i,j,k}(x) = |detP|^{i/2} \Psi\left(Q^j P^i x - k\right) : i, j \in \mathbb{Z} \text{ and } k \in \mathbb{Z}^2 \tag{18}$$

Were,

$\Psi \in L^2(\mathbb{Z}^2)$, P and Q are the 2×2 reversible matrices that represent dilation and geometric transform, respectively, and can be written as:

$$P = \begin{pmatrix} a & 0 \\ 0 & \sqrt{a} \end{pmatrix}, \quad P = \begin{pmatrix} 1 & s \\ 0 & 1 \end{pmatrix}$$

Thus, the DST for each mother function Ψ, can be expressed as:

$$SH\{\Psi_{i,j,k} = 2^{(3/4)i} \Psi\left(Q_j P_i - k\right) : i, j \in \mathbb{Z} \text{ and } k \in \mathbb{Z}^2 \tag{19}$$

The tiling of the frequency plane, demonstrating its multi-scale directional structure, whereas $\xi = (\xi_1, \xi_{2)} \in \mathbb{Z}^2$ indicates the variables in the frequency plane. The Shearlet transform has the advantage of dividing the frequency space step by step, which improves its efficiency. Furthermore, the DST may generate a set of basic functions by combining the scale, rotation, and transform. This benefit stems from the advantages of the DST over the wavelet transform. On a trapezoid-like pair, each element of $\Psi_{a,s,t}$ has frequency support.

D. SCHUR DECOMPOSITION
The Real Schur decomposition is basically known as Schur Decomposition (SD). The SD of a real square matrix X, i.e., $X \in \mathbb{R}^{n \times n}$ is in three matrices Q, U, and the transpose of Q, $Q \in \mathbb{R}^{n \times n}$ as follows.

$$X = Q * U * Q^T \tag{20}$$

Were,

Q is a unitary matrix
Q^T is transposed matrix of Q
U is a quasi-triangular matrix.

The scalar diagonal of the Matrix U has the real eigenvalues, and the 2×2 blocks on the diagonal have the complex eigenvalue.

The fruitful use of SVD in digital image watermarking indicates that Schur decomposition might be used for the same reason because it is a significant intermediary step in the SVD decomposition [26]. The SD requires only one-third of the calculations needed for SVD decompositions [27].

E. LIFTING WAVELET TRANSFORM
LWT (Lifting Wavelet Transform) is an integer to integer transform designed to reduce computational complexity [28], [29]. Noise reduction, compression, and watermarking are the applications of the LWT transformations. When Shearlet transform and LWT transforms are coupled in the watermarking scheme, they can significantly improve the

robustness of the scheme. In 2-Dimensional LWT transform image is run through two high-pass and low-pass filters in both vertical and horizontal directions. It produces four frequency sub-bands, denoted by the LL, LH, HL, and HH. While the resolution of the LL frequency sub-band is strong, the resolution of the three high-frequency sub-bands is low. The information can be included in the correct coefficients created by LWT, which is one of the advantages of using LWT rather than DWT in the proposed technique. When performing the process of coefficient recovery using inverse LWT, the amount of information retrieval error that occurs is lower as a percentage. It helps in the process of restoring the image from its original state. The following three processes make up the construction of a signal of the lifting scheme:

- **Split** – During the split phase, the provided signal $\xi(i)$ is separated into non-overlapping sets, i.e., odd $\xi_o(i)$ and even $\xi_e(i)$

$$\xi_e(i) = \xi(2i), \quad \xi_o(i) = \xi(2i+1) \tag{21}$$

- **Predict** – This phase predicts an odd set from the even set. The predicted phase compensates for the polynomial components that occur in the high pass. Now odd sets $\xi_o(i)$ are predicted using an even set $\xi_e(i)$ and the difference $\varphi(i)$ is produced as

$$\varphi(i) = \xi_o(i) - P_r[\xi_e(i)], \tag{22}$$

In the above equation, P_r [.] denotes the prediction operator, and $\varphi(i)$ represents a high-frequency component. $\varphi(i)$ represents the difference in accuracy between the actual set and the predicted value.

- **Update** -To determine the scaling function, the even set $\xi_e(i)$) is updated using the wavelet coefficient. Thus, this phase is sometimes referred to as the low-pass filtering operation phase. An approximation of the original signal $\xi(i)$ is denoted by the variable $L(i)$, which is defined as

$$L(i) = \xi_e(i) + U_p[\varphi(i)] \tag{23}$$

F. AFFINE TRANSFORM
It is common practice to employ affine transformation to accomplish the reversible transformation of integers [1]. Compared to previous ways of scrambling, it enables the selection of a greater number of parameters during the scrambling process. A further advantage of affine transformations is that it can produce an excellent scrambling effect with only a few cycles of the effect being applied. In this way, to encrypt the watermark, the affine transform is utilized to improve the watermark's level of security. The private integer key $\mathcal{K}$ determines the number of possible transformations. An affine transform is the combining of translation with other nonsingular linear transformations. It is defined as equation (24)

$$\begin{pmatrix} P' \\ Q' \end{pmatrix} = \begin{cases} M \times \left(\dfrac{P}{Q}\right) + \begin{pmatrix} i \\ j \end{pmatrix}, & if\ P < Q - 1 \\ M \times \left(\dfrac{P}{Q}\right) + \begin{pmatrix} 1 \\ j \end{pmatrix}, & if\ P \geq Q - 1 \end{cases} \tag{24}$$

where the original position of the pixel is denoted by $\left(\frac{P}{Q}\right)$ and the encrypted position of the pixel is denoted by $\left(\frac{P'}{Q'}\right)$, all translation transformations are denoted by $\left(\frac{i}{j}\right)$ and $\left(\frac{1}{j}\right)$, matrix M is the affine matrix, and e and f are constants.

Since the affine transform matrix, M is a nonsingular matrix, and its inverse matrix is assumed to be M^{-1}, where L is the length of the image, the inverse transformation equation for the affine transform can be written as follows: (25)

$$\left(\frac{P}{Q}\right) = \begin{cases} M^{-1} \times \left(\frac{P'}{Q'}\right) - M^{-1} \times \left(\frac{i}{j}\right), \\ \quad if\ P' + Q' \leq L + 1 \\ M^{-1} \times \left(\frac{P'}{Q'}\right) - M^{-1} \times \left(\frac{1}{j}\right), \\ \quad if\ P' + Q' > L + 1 \end{cases} \quad (25)$$

III. PROPOSED METHODOLOGY

This section proposes watermarking in the Shearlet domain using LWT and affine transform for lung CT-Scan in NIfTI image format content authentication. The most proposed watermarking schemes have been developed for the.jpg,.bmp,.tiff, etc., medical image format. In the initial phase (Slice Selection Phase), Otsu's image binarization and thresholding method for lung segmentation select the appropriate slice of the NIfTI image to embed the watermark. The watermark is embedded into the selected slice in the second phase (Watermark Embedding Phase). A watermarking scheme consists of two procedures: Watermark embedding and watermark extraction. The proposed scheme satisfies the watermarking system's requirements. Furthermore, image selection has been made using Otsu's image binarization and thresholding method. The hybrid combination of SWT, LWT, and affine transform improves the robustness of the watermarking scheme. These watermarking processes are described as follows.

A. NIFTI IMAGE PRE-PROCESSING

Slice selection from the multiple slices of the NIfTI image has been accomplished in this section. Segmentation is the process of splitting an image into distinct parts based on similar characteristics. Segmentation plays a vital role in selecting an appropriate slice of the NIfTI image for watermark insertion. A watermark must be inserted in that slice which contains less information about the lung. The segmentation has been carried out using Otsu's threshold technique in the proposed scheme because of its consistency and efficacy. Every slice has two distinct parts: foreground and background. This method aims to determine the threshold value for those locations in the slice where the foreground and background expansion are minimal. Fig. 2 depicts the segmentation steps of the proposed scheme, and Fig. 3 shows the mean pixel thresholding for binarization and applies some morphological operations to get the connect component. Finally, get the largest region of the binary image.
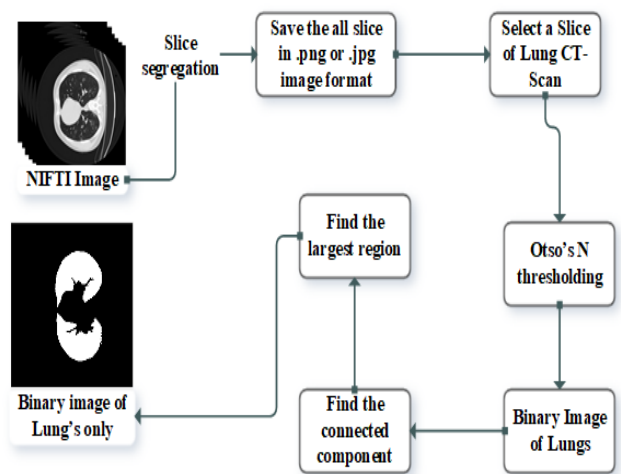

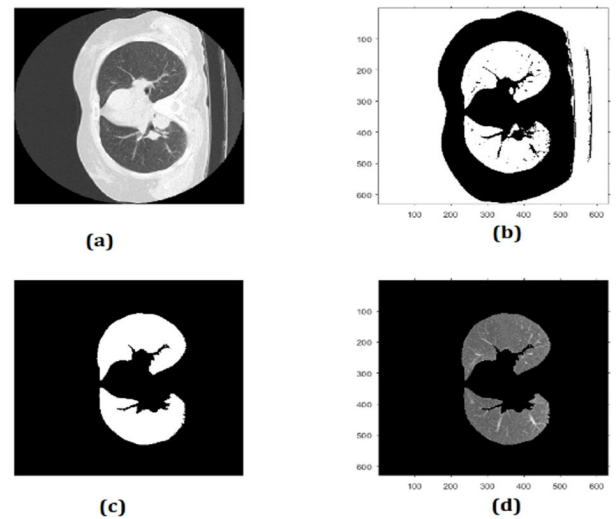**FIGURE 2.** Process diagram for binary image generation of only lung's region.

FIGURE 3. (a) Original slice of NIfTI image (b) Binarization performed on slice (c) Morphological operation performed (d) Segmented lung's slice.

The process of selecting the slice for watermarking will now begin. We prefer the slice with the least amount of medical information about the lung's region for watermark insertion. Select the image with the highest slice position in the NIFTI image array file format if multiple slices have the same amount of data. The otsu's algorithm described above was applied to each slice of the NIfTI image to generate a binary image of the segmented lungs.

To determine which slice contains less information and which contains more information. Find the number of black pixels in each segmented binary image and select the one which contains the highest number of black pixels. If there are multiple-segmented binary images with an equal number of highest black pixels, select the image with the highest slice position in the NIFTI image array file format. This procedure has been applied to all the NIfTI images used in
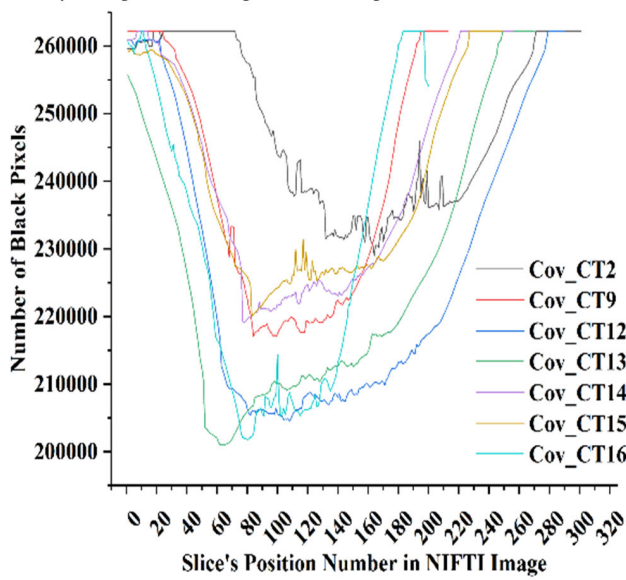
the experiment. Fig. 4 depicts the number of black pixels in each segmented binary image of the lung in each NIfTI image with slice dimension 512 × 512. Fig. 4 show that the some beginning and ending slices of the NIfTI image have the maximum black pixels. These black pixels represent the slice's non-lungs region.

B. WATERMARK EMBEDDING PROCEDURE

The process of embedding the watermark is going to be covered in this section. A binary watermark is embedded in the selected slice of the NIfTI image (the slice selection method has been discussed in the NIfTI image preprocessing section). After successfully identifying the host slice position in the NIfTI image for watermarking, we can begin the watermark embedding process. This process first separated the patient's metadata from the NIfTI image and preserved it securely. Now DST is applied to the image that decomposes it into the approximate and details shear. After that, approximate shear is subjected to LWT, separating it into low and high-frequency bands (LL, HL, HH, LH) and dividing the LL band into 4 × 4 non-overlapping blocks. Now Schur decomposition is applied over these blocks, which decomposes them into three matrixes $Q \times U \times Q^T$. We use the affine transform for watermark encryption, which provides more robustness. After the encryption generates the complete binary sequence of the watermark. Finally, the watermark's bit is embedded in the largest element (U_{max}) of U matrix of the selected blocks using the equation (30). Repeat this process until all the bits are not embedded. In the last step, the watermarked slice and the other slices, along with the information on the patient, are integrated to produce the watermarked NIfTI image. This process is detailed below:

Input: NIfTI image $\mathfrak{I}$
Watermark $\mathcal{W}$

Step 1. Segregate meta information and select the slice $\mathcal{S}$ as per the above discussion from the image.

Step 2. Perform DST on the selected slice $\mathcal{S}$

$$DST(\mathcal{S}) = [Approximate\ Shear\ (AS),\ Details\ Shear(DS)] \tag{26}$$

Step 3. Using eq. (1), apply LWT on the approximate Shear (AS).

$$LWT[AS] = [LH, HL, LL, HH] \tag{27}$$

Step 4. Divide the LL band into 4 × 4 non-overlapping blocks.

Step 5. Apply the Schur decomposition on these blocks $\mathcal{B}$ using eq. (13). So, we get three matrixes $Q \times U \times Q^T$

$$Schur(\mathcal{B}) = Q \times U \times Q^T \tag{28}$$

Step 6. Perform Affine Transform (AT) on watermark using the key $\mathcal{K}$ using eq. (14).

$$W' = AT(\mathcal{W}) \tag{29}$$

Step 7. Transformed watermark bits are embedded in the maximum eigenvalue on the diagonal (U_{dig_max}) of **U** matrix of the selected blocks using the following equation

$$U'_{dig\_max}$$
$$= \begin{cases} U_{dig\_max} - mod\left(U_{dig\_max}, \mathbf{Z}\right) + 0.75 \times \mathbf{Z}, \\ \quad\quad if\ \mathcal{W} = 1 \\ U_{dig\_max} - mod\left(U_{dig\_max}, \mathbf{Z}\right) + 0.25 \times \mathbf{Z}, \\ \quad\quad if\ \mathcal{W} = 0 \end{cases} \tag{30}$$

where Z is the quantization step using key K_z.

Step 8. Perform inverse Schur decomposition. (31).

$$LL_{mod} = Q \times U' \times Q^T \tag{31}$$

Step 9. Perform inverse LWT transform using the following equation

$$AS' = ILWT[LL_{mod}, LH, HL, HH] \tag{32}$$

Step 10. Perform inverse DST using the following equation

$$B' = IDST[LL', LH, HL, HH] \tag{33}$$

Step 11. Step-5 to step-8 is repetitively performed to embed all the watermark bits.

Step 12. To generate the final watermarked NIfTI image, we combined the patient's metadata and other slices with the watermarked slice.

The above-discussed watermarking steps can be applied to any slice of the NIfTI image for watermark embedding. If someone is more frightened about security, they can insert the watermark in the multiple slices of the NIfTI image. The experiment to prove the superiority of the proposed watermarking approach.

C. WATERMARK EXTRACTION PROCESS

After successfully embedding the watermark, we must obtain the embedded watermark from the medical image to validate the image before diagnosis. So, the watermark extraction process starts with selecting the slice used for watermarked embedding from the watermarked NIfTI image (the slice selection process has been discussed above). Initially, we applied the DST and selected the approximate shear for further processing. The next step, apply the LWT, and then the LL band is divided into 4×4 blocks. We apply the Schur decomposition on each block and extract the bits that make up the watermark from the upper triangular matrix U using the equation (37). The affine transform is applied to the bits recovered from the upper triangular matrix to create the watermark in the last step. The proposed watermark extraction approach is described in more detail below.

Input: Watermarked NIfTI image $\mathfrak{T}'$
Output: Extracted Watermark
Step 1. Select the watermarked slice $\mathcal{S}'$.
Step 2. Perform one level DST on the block $\mathcal{B}$

$$DST\,(B) = [Approximate\ Shear\,(AS)\,, Details\ Shear(DS)]$$
(34)

Step 3. Apply LWT on the Approximate Shear (AS) band using eq. (1).

$$LWT\,(AS) = [LH^*, HL^*, LL^*, HH^*] \qquad (35)$$

Step 4. Divide the LL^* band into 4×4 non-overlapping blocks $\mathcal{B}^*$.
Step 5. Apply the Schur decomposition on the $\mathcal{B}^*$ band using eq. (13). So, we get three matrixes $Q \times U' \times Q^T$

$$Schur\,(\mathcal{B}^*) = Q \times U' \times Q^T \qquad (36)$$

Step 6. Select the largest element U'_{max} from the Schur matrix U'. Use the following equation and key K_z for watermark extraction

$$\mathfrak{B} = \begin{cases} 0, & if\ mod\left(U'_{dig\_max}, Z\right) < 0.5 \times Z \\ 1, & else \end{cases} \qquad (37)$$

Step 7. Finally, decrypt the watermarking using the inverse affine transform (IAT) on the extracted bits using the key to generate the watermark.

$$W' = IAT\,(\mathfrak{B}) \qquad (38)$$

IV. EXPERIMENTAL RESULTS & PERFORMANCE ANALYSIS

A. PERFORMANCE EVALUATION METRICS

The suggested watermarking method is evaluated using PSNR, Q, SSIM, and NC [19]. PSNR, Q, and SSIM are used to evaluate the imperceptibility of the watermarked slice.

$$PSNR = 10 * \log_{10} \frac{(Max)^2}{\frac{1}{m*n} \sum_{i=0}^{m} \sum_{j=0}^{n} \left(A_{ij} - B_{ij}\right)^2} \qquad (39)$$

To evaluate how similar the original slice and the watermarked slice are to one another, the SSIM is used. The value
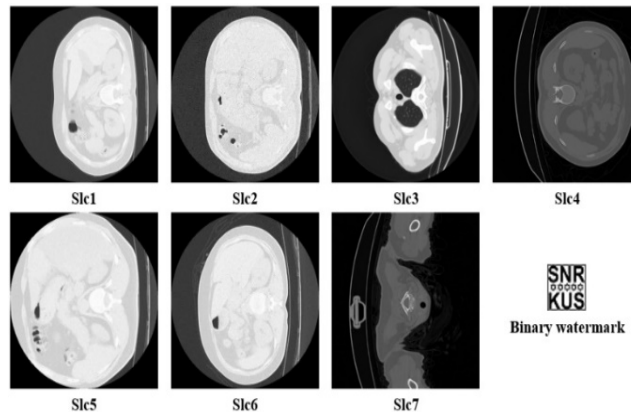

FIGURE 5. Slices of NIfTI image (Slc1 to Slc7) used for experimental analysis and watermark.

TABLE 1. Results of the proposed scheme without any attacks.

Slices	NC	Q	PSNR	SSIM	Extracted Watermark
Slc1	1	0.9996	60.91	0.9934	
Slc2	0.9998	0.9995	59.98	0.9876	
Slc3	1	1	61.02	0.9951	
Slc4	1	0.9991	59.79	0.9862	
Slc5	1	1	61.12	0.9948	
Slc6	0.9996	0.9998	59.83	0.9855	
Slc7	1	0.9997	60.95	0.9875	

of SSIM can vary from -1 to $+1$; if SSIM is equal to 1, then the original slice and the watermarked slice are the same. The SSIM is computed by using the equation (29)

$$SSIM\,(x, y) = \frac{(2\mu_x\mu_y + c_1)(2\sigma_{xy} + c_2)}{\left(\mu_x^2 + \mu_y^2 + c_1\right)(\sigma_x^2 + \sigma_y^2 + c_2)} \qquad (40)$$

Estimating the degree of similarity between the host slice and the generated watermarked slice is necessary to evaluate how resistant the proposed method is. This is done with the help of the NC parameter. If the NC value is quite near to one, the solution provided is effective in terms of recovery strength. NC computation is given as eq. (30).

$$NC = \frac{\sum_{x=1}^{M} \sum_{y=1}^{N} w\,(x, y) \times w * (x, y)}{\sum_{x=1}^{M} \sum_{y=1}^{N} w^2(x, y)} \qquad (41)$$

B. RESULTS ANALYSIS

Experiments were conducted to test the watermarking scheme's visual quality, integrity, invisibility, and robustness. Invisibility is the ability to hide a watermark without affecting

TABLE 2. Comparsion of PSNR with other exiting technique.

Image	Kumar & Singh [34]	Balasamy & Suganyadevi [17]	Singh et al. [14]	Zhang et al. [2]	Boussif et al. [6]	Kumar et al. [13]	Singh et al. [12]	Bamal et al. [20]	Proposed Scheme
	FRT	DWT	LWT	IWT	FFT	LWT	LWT & MSVD	FWH	DST & LWT
Img1	52.61	49.419	56.76161	51.24	41.3287	54.36	46.98	53.8014	60.91
Img2	52.91	49.357	56.92657	50.19	40.0817	53.83	46.38	54.0554	59.98
Img3	52.82	49.513	57.27539	49.37	35.7515	54.34	46.94	54.5383	61.02
Img4	51.75	49.309	57.06924	50.66	44.5799	54.33	46.88	53.7501	59.79
Img5	51.66	49.201	56.82357	51.21	39.7249	54.38	46.92	53.8454	61.12
Img6	52.68		56.98985		36.8401	54.37	46.91	52.8659	59.83
Img7			56.95649		38.3972			49.6742	60.95
Img8			57.27628		40.8976			53.6426	
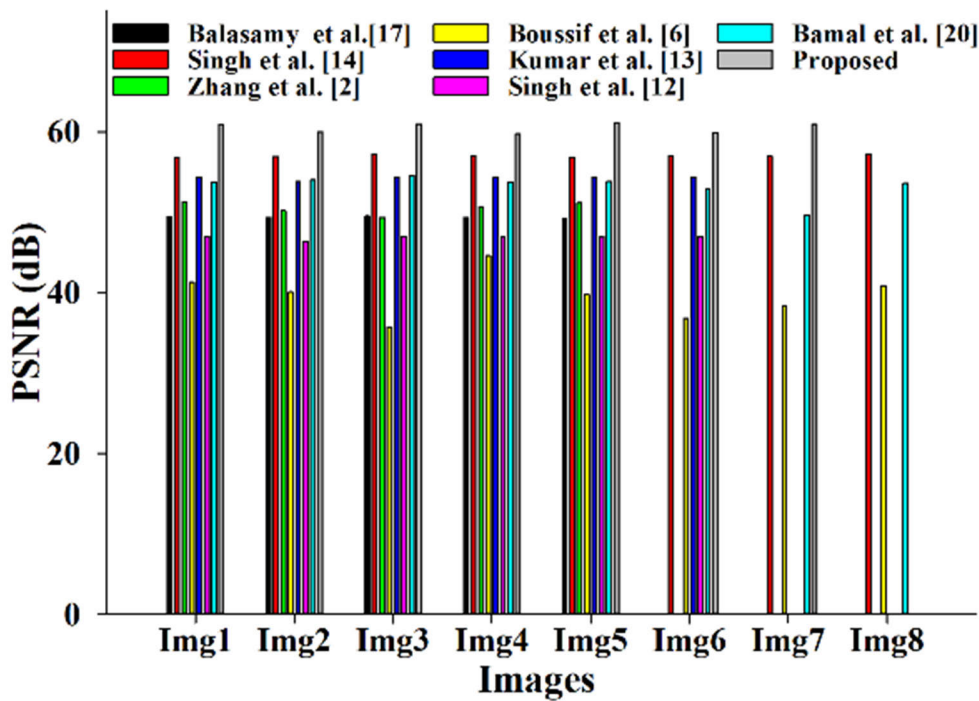
FIGURE 6. PSNR comparison with other existing schemes.

image quality. PSNR determines invisibility. Slc1 to Slc7 are used for watermark insertion and extraction from 7 NIfTI images taken from open database [30]. Fig. 5 shows slices and the watermark used for the experiment where each slice of NIfTI image is 512 × 512, and the watermark size is 32×32. Table 1 shows the experimental result without any attack where the PSNR of the proposed strategies is lies between 59 to 62 dB, NC values are one or near to one, and SSIM is also near to one, proving the excellent imperceptibility of the developed method. The quantization phase is crucial to the operation carried out during the proposed approach. Regarding the determination of the quantization step, Z. If the quantization step increase, the NC value goes up while the SSIM value goes down; this indicates that the imperceptibility has improved while the robustness has been compromised. In light of this, one must consider the trade-off between imperceptibility and resilience. The

proposed technique uses the threshold value of 70 for the quantization step for the experiment.

C. COMPARISON WITH EXISTING SCHEMES

The findings of these comparisons make it clear that the proposed method has achieved remarkable success in producing a watermarked image of good quality. Fig. 6 compares the PSNR of the proposed methodology with various currently available techniques. In this comparison watermark size of the proposed scheme is 32×32, whereas Balasamy et al. [17], Singh et al. [14], Kumar et al. [3], Bamal et al. [20], and Singh et al. [12] also use the same size watermark. Zhang et al. [2] and Boussif [6] embedded a patient's information and medical report, respectively. The comparison reveals that the results obtained using our method were significantly more substantial than other currently available strategies [39], [40].

TABLE 3. Different noise attacks on different variances.

Name of Attack	Variance	Extracted Watermark	NC
Salt and pepper noise	0.001		0.99623
	0.003		0.98935
	0.005		0.97184
Gaussian noise	0.001		0.98254
	0.003		0.96964
	0.005		0.95245
Speckle noise	0.001		0.99014
	0.003		0.97982
	0.005		0.96534

TABLE 4. Extracted watermarks and their NC after JPEG compression attack with the different quality factor.

Quality Parameters	Extracted Watermarks	NC
70		0.99896
60		0.99146
50		0.98954
40		0.97214

TABLE 5. Filter attacks with different window sizes.

Attack	Strength	Extracted Watermark	NC
Median filter	3×3		0.97213
	4×4		0.91547
	5×5		0.88126
Gaussian Low-pass filter	3×3		0.99145
	4×4		0.95424
	5×5		0.91682
Average filter	3×3		0.98246
	4×4		0.93563
	5×5		0.89257

TABLE 6. Performance against the histogram equalization, sharpening, and motion blur attacks.

Name of Attack	Extracted Watermark	NC of Extracted Watermark
Histogram equalization		0.77455
Sharpening (0.2)		0.97478
Motion blur (0.2)		0.85561

D. ROBUSTNESS ANALYSIS

The above data shows that our technique produced significant results on several slices of diverse NIfTI images. Our technique's robustness is demonstrated against various image processing threats. The watermarked slice has been tainted by the addition of various sorts of noise, including salt-and-pepper noise, compression, Gaussian noise, speckle noise, and motion blur. After an attack, a watermark is retrieved, and the NC values of extracted watermarks are given in tables against unintended attacks. The quality of the retrieved watermarks was lowered but still adequate under particular attacks. Table 3 shows the results of salt-and-pepper, speckle, and Gaussian noise, wherein NC is more significant for each attack. Therefore, the proposed scheme performs well against noise attacks.

JPEG compression is applied over the watermarked slice with different quality factors of 40, 50, 60, and 70, and the embedded watermark was adequately recovered. This attack is shown for the NIfTI images in Table 4, and the data indicate that the effectiveness of the proposed scheme is promising.

Now we have applied the different types of image filtering attacks with different window sizes, i.e., 3 × 3, 4 × 4, and 5 × 5, and the results are shown in Table 5. When median filter, Gaussian Low-pass filter, and Average filter attack on the watermark slice with these window sizes, they extract the watermark with good NC values closer to one.

Table 6 shows the NC of the extracted Watermark after the histogram equalization, sharpening, and Motion blur attacks. The proposed scheme performs the average against the histogram equalization and motion blur but performs well against the sharpening where the NC value is near one.

V. CONCLUSION

The fast expansion of the internet has made medical facilities more accessible using telemedicine applications. In this Covid-19 epidemic crisis, remote radiology has become extremely popular and beneficial within many radiology organizations and healthcare centers worldwide. Teleradiology has benefited these organizations due to technological advancements, a scarcity of experienced radiologists, and the necessity for better diagnostic services. Medical data sharing with radiologists over the internet may be tampered

with, leading to inaccurate diagnosis and image integrity loss. To overcome the problems and enhance efficiency, this paper presented a watermarking scheme for NIfTI images based on Shearlet transform, LWT, and affine transform with the help of Otus' image binarization and segmentation. The resilient watermark is integrated with the approximation and detailed coefficients of Shearlet-based LWT and Schur decomposition, respectively, significantly improving the scheme's imperceptibility and resilience. Meanwhile, the affine transform ensures the algorithm's security and reliability.

The watermark is extracted with the highest possible correlation under multiple attacks. The experimental results show that the proposed scheme is superior and more efficient than the existing schemes discussed in the literature regarding image quality and robustness against various attacks. The proposed scheme is efficient and secure for NIfTI image authentication according to the benefits. In the future, we will explore alternative medical image formats, such as Analyze and Minc., for watermarking.

ACKNOWLEDGMENT

REFERENCES

[1] B. Hu, "Characteristics of SARS-CoV-2 and COVID-19," *Nature Rev. Microbiol.*, vol. 19, no. 3, pp. 141–154, 2021.

[2] X. Zhang, W. Zhang, W. Sun, T. Xu, and S. K. Jha, "A robust watermarking scheme based on ROI and IWT for remote consultation of COVID-19," *Comput., Mater. Continua*, vol. 64, no. 3, pp. 1435–1452, 2020.

[3] M. Larobina and L. Murino, "Medical image file formats," *J. Digit. Imag.*, vol. 27, no. 2, pp. 200–206, Apr. 2014.

[4] Z. Cui, S. Zhong, P. Xu, Y. He, and G. Gong, "PANDA: A pipeline toolbox for analyzing brain diffusion images," *Frontiers Hum. Neurosci.*, vol. 7, p. 42, Feb. 2013.

[5] K. Balasamy and S. Suganyadevi, "A fuzzy based ROI selection for encryption and watermarking in medical image using DWT and SVD," *Multimedia Tools Appl.*, vol. 80, no. 5, pp. 7167–7186, Feb. 2021.

[6] M. Boussif, N. Aloui, and A. Cherif, "DICOM imaging watermarking for hiding medical reports," *Med. Biol. Eng. Comput.*, vol. 58, no. 11, pp. 2905–2918, Nov. 2020.

[7] A. F. Qasim, R. Aspin, F. Meziane, and P. Hogg, "ROI-based reversible watermarking scheme for ensuring the integrity and authenticity of DICOM MR images," *Multimedia Tools Appl.*, vol. 78, no. 12, pp. 16433–16463, Jun. 2019.

[8] A. Al-Haj, "Providing integrity, authenticity, and confidentiality for header and pixel data of DICOM images," *J. Digit. Imag.*, vol. 28, no. 2, pp. 179–187, Apr. 2015.

[9] H.-T. Hu, L.-Y. Hsu, and H.-H. Chou, "An improved SVD-based blind color image watermarking algorithm with mixed modulation incorporated," *Inf. Sci.*, vol. 519, pp. 161–182, May 2020.

[10] A. Mohanarathinam, "Digital watermarking techniques for image security: A review," *J. Ambient Intell. Humanized Comput.* vol. 11, no. 8, pp. 3221–3229, 2020.

[11] Q. Su, D. Liu, and Y. Sun, "A robust adaptive blind color image watermarking for resisting geometric attacks," *Inf. Sci.*, vol. 606, pp. 194–212, Aug. 2022.

[12] K. U. Singh, H. S. Abu-Hamatta, A. Kumar, A. Singhal, M. Rashid, and A. K. Bashir, "Secure watermarking scheme for color DICOM images in telemedicine applications," *Comput., Mater. Continua*, vol. 70, no. 2, pp. 2525–2542, 2022.

[13] A. Kumar, K. U. Singh, V. D. A. Kumar, T. Kant, A. K. J. Saudagar, A. A. Tameem, M. A. Khathami, M. B. Khan, M. H. A. Hasanat, and K. M. Malik, "Robust watermarking scheme for NIfTI medical images," *Comput., Mater. Continua*, vol. 71, no. 2, pp. 3107–3125, 2022.

[14] K. U. Singh, A. Kumar, T. Singh, and M. Ram, "Image-based decision making for reliable and proper diagnosing in NIFTI format using watermarking," *Multimedia Tools Appl.*, vol. 81, no. 27, pp. 39577–39603, Nov. 2022.

[15] F. Ernawan, A. Aminuddin, D. Nincarean, M. F. A. Razak, and A. Firdaus, "Three layer authentications with a spiral block mapping to prove authenticity in medical images," *Int. J. Adv. Comput. Sci. Appl.*, vol. 13, no. 4, pp. 211–223, 2022.

[16] J. Gao, Z. Li, and B. Fan, "An efficient robust zero watermarking scheme for diffusion tensor-magnetic resonance imaging high-dimensional data," *J. Inf. Secur. Appl.*, vol. 65, Mar. 2022, Art. no. 103106.

[17] M. S. Moad, M. R. Kafi, and A. Khaldi, "Medical image watermarking for secure e-healthcare applications," *Multimedia Tools Appl.*, vol. 81, no. 30, pp. 44087–44107, Dec. 2022.

[18] M. M. Sayah, K. M. Redouane, and K. Amine, "Secure transmission and integrity verification for color medical images in telemedicine applications," *Multimedia Tools Appl.*, vol. 81, no. 30, pp. 43613–43638, Dec. 2022.

[19] Z. Dai, C. Lian, Z. He, H. Jiang, and Y. Wang, "A novel hybrid reversible-zero watermarking scheme to protect medical image," *IEEE Access*, vol. 10, pp. 58005–58016, 2022, doi: 10.1109/ACCESS.2022.3170030.

[20] R. Bamal and S. S. Kasana, "Dual hybrid medical watermarking using Walsh-slantlet transform," *Multimedia Tools Appl.*, vol. 78, no. 13, pp. 17899–17927, Jul. 2019.

[21] K. U. Singh, S.-Y. Hsieh, C. Swarup, and T. Singh, "Authentication of NIfTI neuroimages using lifting wavelet transform, Arnold cat map, Z-transform, and Hessenberg decomposition," *Traitement Signal*, vol. 39, no. 1, pp. 265–274, Feb. 2022.

[22] B. Kurt, V. V. Nabiyev, and K. Turhan, "A novel automatic suspicious mass regions identification using Havrda & Charvat entropy and Otsu's N thresholding," *Comput. Methods Programs Biomed.*, vol. 114, no. 3, pp. 349–360, May 2014.

[23] M. T. Nyo, "Otsu's thresholding technique for MRI image brain tumor segmentation," *Multimedia Tools Appl.*, vol. 2022, pp. 1–13, May 2022.

[24] L. Zhou, M.-J. Zuo, H. Shi, Y. Zhang, and L.-H. Gong, "Robust watermarking algorithm against the geometric attacks based on non-subsampled shearlet transform and Harris-Laplace detector," *Secur. Commun. Netw.*, vol. 2022, pp. 1–14, Mar. 2022.

[25] M. N. Favorskaya, L. C. Jain, and E. I. Savchina, "Perceptually tuned watermarking using non-subsampled shearlet transform," in *Computer Vision in Control Systems-4*. Cham, Switzerland: Springer, 2018, pp. 41–69.

[26] G. H. Golub and C. F. Van Loan, *Matrix Computations*. Baltimore, MD, USA: Johns Hopkins University Press, 1989.

[27] Q. Su, Y. Niu, X. Liu, and Y. Zhu, "Embedding color watermarks in color images based on Schur decomposition," *Opt. Commun.*, vol. 285, no. 7, pp. 1792–1802, Apr. 2012.

[28] W. Sweldens, "The lifting scheme: A construction of second generation wavelets," *SIAM J. Math. Anal.*, vol. 29, no. 2, pp. 511–546, Mar. 1998.

[29] W. Sweldens, "The lifting scheme: A custom-design construction of biorthogonal wavelets," *Appl. Comput. Harmon. Anal.*, vol. 3, no. 2, pp. 186–200, Apr. 1996.

[30] J. Ma, G. Cheng, W. Yixin, A. Xingle, G. Jiantao, Y. Ziqi, and J. He. (2020). *COVID-19 CT Lung and Infection Segmentation Dataset (Version 1.0) [Data Set]*. Zenodo. [Online]. Available: https://zenodo.org/record/3757476#.Y4ayQnZBzIU

[31] D. Li, Y. Chen, J. Li, L. Cao, U. A. Bhatti, and P. Zhang, "Robust watermarking algorithm for medical images based on accelerated-KAZE discrete cosine transform," *IET Biometrics*, vol. 11, no. 6, pp. 534–546, Nov. 2022.

[32] Z. Liu, J. Li, Y. Ai, Y. Zheng, and J. Liu, "A robust encryption watermarking algorithm for medical images based on ridgelet-DCT and THM double chaos," *J. Cloud Comput.*, vol. 11, no. 1, pp. 1–20, Oct. 2022.

[33] Z. Zhang, F. Li, X. Zuo, Q. Meng, and S. Jin, "Reversible image watermarking algorithm based on reverse histogram translation," *Multimedia Tools Appl.*, vol. 2022, pp. 1–15, Sep. 2022.

[34] L. Kumar and K. U. Singh, "Color ultrasound image watermarking scheme using FRT and Hessenberg decomposition for telemedicine applications," *JUCS-J. Universal Comput. Sci.*, vol. 28, no. 9, pp. 882–897, Sep. 2022, doi: 10.3897/jucs.94127.

[35] C. Gong, "Robust medical zero-watermarking algorithm based on Residual-DenseNet," *IET Biometrics*, vol. 11, no. 6, pp. 1–10, 2022.

[36] F. Horasan, M. A. Pala, A. Durdu, A. Akgül, Ö. F. Akmeşe, and M. Z. Yıldız, "DWT-SVD based watermarking for high-resolution medical holographic images," *Complexity*, vol. 2022, pp. 1–21, Aug. 2022.

[37] R. G. Babukarthik, D. Chandramohan, D. Tripathi, M. Kumar, and G. Sambasivam, "COVID-19 identification in chest X-ray images using intelligent multi-level classification scenario," *Comput. Electr. Eng.*, vol. 104, Dec. 2022, Art. no. 108405.

[38] A. Kumar, K. Sharma, H. Singh, S. G. Naugriya, S. S. Gill, and R. Buyya, "A drone-based networked system and methods for combating coronavirus disease (COVID-19) pandemic," *Future Gener. Comput. Syst.*, vol. 115, pp. 1–19, Feb. 2021.

[39] A. Kumar, K. Sharma, H. Singh, P. Srikanth, R. Krishnamurthi, and A. Nayyar, "Drone-based social distancing, sanitization, inspection, monitoring, and control room for COVID-19," in *Artificial Intelligence and Machine Learning for COVID-19*. Cham, Switzerland: Springer, 2021, pp. 153–173.

[40] S. Jain, P. Chawla, K. Kaushik, and A. Kumar, "Technologies for vaccinating COVID-19, its variants and future pandemics: A short survey," in *Artificial Intelligence, Machine Learning, and Mental Health in Pandemics*. New York, NY, USA: Academic, 2022, pp. 299–341.

ANKIT KUMAR received the B.Tech. degree in computer science and engineering from West Bengal Technical University, Kolkata, in 2010, and the M.Tech. degree in computer science engineering and the Ph.D. degree in computer science from the Indian Institute of Information technology, Allahabad (IIIT Allahabad), India, in 2012 and 2022, respectively. He is currently working as an Assistant Professor with the Department of Computer Engineering and Application, GLA University, Mathura. He developed optimization algorithms in machine learning and data science. He has word on optimization problems especially in medical applications. He has published more than 70 research papers in reputed journals and conferences in high indexing databases and granted nine patents from Australia and India. He has authored two edited books published by Apple Publisher and CRC Press. He has completed one funded research projects from the TEQIP-3. His current research interests include machine learning, deep learning, big data, and evolutionary computation and its application in real-world. He is an Associate Editor for reputed journals and publishers, such as *Traitement du Signal*, *Ingénierie des Systèmes d'Information* (ISI), *International Journal of Cyber-Physical Systems* (IJCPS), and *Journal of Information Technology Research* (JITR). He also serves as a Reviewer for several journals, including the IEEE TRANSACTIONS, *ACM Transactions*, IEEE ACCESS, and *Multimedia Tools and Applications*.

KAMRED UDHAM SINGH received the Ph.D. from Banaras Hindu University, India, in 2019. From 2015 to 2016, he was a Junior Research Fellow with University Grant Commission (UGC), India. From 2017 to 2019, he was a Senior Research Fellow with UGC. In 2019, he became an Assistant Professor with the School of Computing, Graphic Era Hill University, India. He is currently a Postdoctoral Fellow at the Department of Computer Science and Information Engineering (CSIE), National Cheng Kung University, Taiwan. His research interests include image security and authentication, deep learning, medical image watermarking, and steganography.

SANDEEP KAUTISH received the bachelor's, master's, and Ph.D. degrees in computer science on intelligent systems in social networks and the master's Diploma degree in management. He is currently working as a Professor and the Director of the LBEF Campus, Kathmandu, Nepal, running in academic collaboration with the Asia Pacific University of Technology and Innovation, Malaysia (#301-350 in QS Asian University Rankings). He is also an academician by choice and backed with more than 18 years of work experience in academics, including over eight years in academic administration in various institutions of India and abroad. He has meritorious academic records throughout his academic career. He has over 60 publications in his account and his research works has been published in reputed journals, such as Springer, Elsevier, Taylor & Francis, Hindawi and IGI Global with high impact factor, and SCI/SCIE/Scopus/WoS indexing. His research interests include healthcare analytics, business analytics, machine learning, data mining, decision support systems, and information systems.

SURBHI BHATIA received the Ph.D. degree in computer science and engineering in the area of machine learning and social media analytics. She is currently an Associate Professor with the Department of Information Systems, College of Computer Sciences and Information Technology, King Faisal University, Saudi Arabia, and also serving as an Academic editor, Associate Editor and Guest editor in reputed journals. She is an Adjunct Professor at Shooing University, Himachal Pradesh, India. She earned Project management Professional Certification from reputed Project Management Institute, USA. She has more than 10 years of Academic and Teaching Experience at Different Universities. She has published many papers in reputed journals and conferences in high indexing outlets and ten international patents from India, Australia, USA, and also authored and edited around 12 books. She has conducted workshops in AICTE programmers and chaired technical sessions in many conferences. She has completed many research funded projects approved at the Ministry of Education, Saudi Arabia, and the Deanship of Scientific Research. Her research interests include information systems, artificial intelligence, and data analytics. She has delivered talks as keynote speaker in IEEE conferences and in a faculty development programs.

ADARSH KUMAR received the M.Tech. degree in software engineering from the Thapar University of Engineering and Technology, Patiala, Punjab, India, the first Ph.D. degree from the Jaypee Institute of Information Technology University, Noida, India, and the second Ph.D. degree from the Software Research Institute, Athlone Institute of Technology, Ireland. From 2005 to 2016, he was with the Department of Computer Science Engineering and Information Technology, Jaypee Institute of Information Technology, where he worked as an Assistant Professor. He is currently an Associate Professor with the School of Computer Science, University of Petroleum and Energy Studies, Dehradun, India. He has many research papers in reputed journals, conferences, and workshops. He has also participated in one European Union H2020-sponsored research project. He is currently executing one research project sponsored by the UPES SEED Division and one sponsored by Lancaster University. His main research interests include cybersecurity, cryptography, network security, and ad-hoc networks.

SHAKILA BASHEER is currently an Assistant Professor with the Department of Information Systems, College of Computer and Information Sciences, Princess Nourah Bint Abdulrahman University, Riyadh, Saudi Arabia. She has worked and contributed in the field of data mining, image processing, and fuzzy logic. She has more than ten years of teaching experience and has published more technical papers in international journals/proceedings of international conferences/edited chapters of reputed publications. Her research interests include data mining algorithms using fuzzy logic, data mining, vehicular networks machine learning, block chain, vehicular networks, and the IoT.

ALAA ALI HAMEED received the master's degree in computer engineering from Eastern Mediterranean University, North Cyprus, in 2012, and the Ph.D. degree from the department of computer engineering, Selcuk University, Turkey, in 2017. From 2017 to 2019, he was worked as an Assistant Professor at the Department of Computer Engineering, Istanbul Aydin University, Turkey, and also he worked as an Assistant Professor at the Department of Computer Engineering, Istanbul Sabahattin Zaim University, Turkey, from 2019 to 2022. He is currently as an Assistant Professor with the Department of Computer Engineering, Istinye University, Turkey. He has published more than 60 technical articles in top international journals and conferences. He served as a Program Chair and a Technical Program Chair member for many international conferences, also he served as a Guest Editor for many SCIE journals. His research interests include digital signal and image processing, adaptive filters, adaptive computing, data mining, machine and deep learning, big data and data analytics, neural networks and self-learning systems, and artificial intelligence.

. . .